Molecular Crystals and Liquid Crystals
Publication details, including instructions for authors and subscription information:
http://www.informaworld.com/smpp/title~content=t713644168

Synthesis, Characterization, and Electro-Optic Properties of Novel Ferroelectric Liquid Crystal with a Large Tilt Angle and Wide Temperature Range of Chiral Smectic C Phase

Chien-Tung Liao[a]; Jiunn-Yih Lee[a]; Chiu-Chun Lai[b]
[a] Department of Polymer Engineering, National Taiwan University of Science and Technology, Taipei, Taiwan, ROC [b] Department of Textile Engineering, Chinese Culture University, Taipei, Taiwan, ROC

First published on: 18 January 2011

To cite this Article Liao, Chien-Tung , Lee, Jiunn-Yih and Lai, Chiu-Chun(2011) 'Synthesis, Characterization, and Electro-Optic Properties of Novel Ferroelectric Liquid Crystal with a Large Tilt Angle and Wide Temperature Range of Chiral Smectic C Phase', Molecular Crystals and Liquid Crystals, 534: 1, 3 — 18
To link to this Article: DOI: 10.1080/15421406.2010.526470
URL: http://dx.doi.org/10.1080/15421406.2010.526470

Mol. Cryst. Liq. Cryst., Vol. 534: pp. 3–18, 2011

ISSN: 1542-1406 print/1563-5287 online
DOI: 10.1080/15421406.2010.526470

Taylor & Francis
Taylor & Francis Group

Synthesis, Characterization, and Electro-Optic Properties of Novel Ferroelectric Liquid Crystal with a Large Tilt Angle and Wide Temperature Range of Chiral Smectic C Phase

CHIEN-TUNG LIAO,[1] JIUNN-YIH LEE,[1] AND CHIU-CHUN LAI[2]

[1]Department of Polymer Engineering, National Taiwan University of Science and Technology, Taipei, Taiwan, ROC
[2]Department of Textile Engineering, Chinese Culture University, Taipei, Taiwan, ROC

The present article is a study of the ferroelectric behavior in low-molar-mass organosiloxane liquid-crystal materials classed. A few novel compounds with large tilt angle and wide temperature range of the SmC phase have been synthesized, and the mesophases exhibited by them have been compared. The mesophases under discussion were investigated by means of polarizing microscopy, differential scanning calorimetry, X-ray diffraction, as well as electro-optical experiments. The influence of the molecular structure on the occurrence of the SmC* phase was investigated. Finally, the electro-optical properties of the SmC* phase, such as tilt angle, dielectric permittivity, and switching behavior, were also measured. As a consequence, the correlation between their electro-optical properties and chemical structures of these compounds is investigated.*

Keywords Chemical reactions; optical microscopy; thermal analysis

Introduction

Ferroelectric liquid-crystal compounds (FLC) of large tilt angle that are useful for high-speed modulation or switching of optical radiation were developed. Such FLC are useful in total internal reflection (TIR) switching devices. When an applied DC voltage rotates the molecules through about a 90° angle, which changes the perceived refractive index at the FLC layer and permits rapid optical switching in such TIR switches. For an FLC material to be useful in tilt angle θ of approximately 45°, since the dipole molecule rotates through an angle of about 2θ upon application of a dc field to the cell. When designing new liquid-crystal molecules with large tilt angle and wide temperature range, it is necessary to have in mind that their mesogenic behavior is strongly influenced by the structure of the rigid molecular core [1].

Address correspondence to Prof. Jiunn-Yih Lee, Department of Polymer Engineering, National Taiwan University of Science and Technology, Taipei, Taiwan, ROC. E-mail: jlee@mail.ntust.edu.tw

During the last few years, several series of ferroelectric liquid-crystalline materials containing a 4-hydroxyphenyl 4′-hydroxybiphenyl-4-carboxylate core and chiral octan-2-ol unit have been synthesized [2] and studied with the aim of obtaining new materials responding to the application demands and contributing to a better understanding of the chemical structure–to–physical property relationship. The addition of an oligomeric siloxane end-group to a calamitic mesogen has been shown to promote lamellar organization and the formation of smectic phases due to the tendency of siloxane and paraffinic groups to nanosegregate into distinct sublayers [3–13], forming a so-called virtual siloxane backbone that enables dopant compatibilization in a way similar to what is achieved with side-chain liquid-crystalline copolymers [14]. In this article, we report the synthesis and characterization of new ferroelectric liquid-crystal material with a 4-hydroxyphenyl 4′-hydroxybiphenyl-4-carboxylate core, chiral octan-2-ol unit, and oligomeric siloxane end-group. We examined the influence of the addition of different lengths of siloxane and achiral alkyl chains in the end-group on the phase transition. Finally, the properties of the smectic C^* phase, such as the spontaneous polarization as a function of temperature, tilt angle, and relative permittivity, have been measured for target compounds.

Experimental

^{1}H Nuclear magnetic resonance (NMR) spectra were recorded on a Bruker Avance-500 spectrometer (500 MHz), using $CDCl_3$ as solvents. Elemental analyses for C and H were performed on a Heraeus Vario EL-III elemental analyzer. The optical textures of mesophases were characterized by polarizing optical microscopy (POM; model Olympus BH5) equipped with a hot stage (Mettler Toledo FP82HT) and a programmable temperature controller (Mettler Toledo FP90 central processor). Temperatures and enthalpies of transitions were determined by differential scanning calorimetry (DSC; model Perkin Elmer Diamond). Powder samples of ca. 3.0 mg were examined at heating and cooling rates of 5°C min^{-1} under a nitrogen atmosphere.

Synchrotron powder X-ray diffraction (XRD) measurements were performed in transmission geometry with synchrotron radiation at beamline BL17A of the National Synchrotron Radiation Research Center (NSRRC), Taiwan, where the X-ray wavelength was 1.33366 Å. The XRD data were collected using a Mar345 image plate detector mounted orthogonal to the beam with sample-to-detector distance of 280 mm. The diffraction signals were accumulated for 10 s. The powder samples were packed into a capillary tube and heated by a heat gun, where the temperature controller is programmable by a PC with a PID feedback system. The scattering angle theta was calibrated by a mixture of silver behenate and silicon. For the 2D XRD patterns, the surface-aligned samples of the mesophases were obtained by very slow cooling (1°C min^{-1}) of a small droplet of the compound from the isotropic melt on a glass plate treated with commercially available homeotropic agent.

Electro-optical investigations were carried out using commercially available liquid-crystal cells with indium tin oxide (ITO) electrodes coated with antiparallel rubbed polyimide (from Mesostate Corp., cell gap = 7.5 μm for active area = 1 cm^2). The sample was filled into the cell in the isotropic phase. A digital oscilloscope (Yokogawa Elect., DL1640) was used in these measurements, and a high-power amplifier was connected to an arbitrary function generator (Tektronix AWG2005). For the switching polarization experiment was measured using a triangular waveform

voltage method under slow cooling from the isotropic phase. A digital oscilloscope was used in these measurements, and a high-power amplifier was connected to a function generator and a dc power supply was utilized in the dc field experiments. During electro-optical measurements, the modulations of textures by applying electric fields were observed using a polarizing optical microscope. Finally, we also measured the complex dielectric permittivity (detected by HP4192A) in the frequency range 10^2–10^7 Hz for the planar-aligned (measuring field is normal to the director) sample on cooling at a rate of about 1°C min^{-1}, keeping the temperature of the sample stable during frequency sweeps.

The pitch experimental setup and the preparation of the sample with planar and homogeneous alignment have been described in detail in a previous paper [15]. The cell thickness was 25 μm. The monodomain chosen for measurement has a dimension of $2 \times 1\,mm^{-2}$. The pitch is measured from the whole length of 30 stripes with a micrometer eye-piece attached to the microscope.

Materials

All reagents and chemicals were purchased from commercial sources (Alfa, TCI, and Fluka) and used as received without further purification. Tetrahydrofuran (THF) and dichloromethane (CH_2Cl_2) were distilled to keep anhydrous before use. Reactions were monitored by thin-layer chromatography (TLC) on silica gel plates (Merck TLC silica gel 60 F_{254} aluminum sheets), which were examined under ultraviolet (UV) light and iodine vapor. Column chromatography was performed using Merck 60-mesh silica gel.

Synthesis

The general synthetic routes of intermediates and target bent-core molecules are shown in Scheme 1. The purity and chemical structures of the intermediates and target compounds can be easily verified by TLC, ^{1}H NMR spectroscopy, and elemental analysis. The synthetic procedures and chemical analyses of each product are described sequentially below.

4-(Benzyloxy) Phenol, ***1***. This compound was prepared according to published procedures [16], as a white solid in 81% yield. ^{1}H NMR (ppm, $CDCl_3$): 4.55 (s, 1H), 5.00 (s, 2H), 6.76 (d, $J = 9.3$ Hz, 2H), 8.87 (d, $J = 9.0$ Hz, 2H), 7.25–7.44 (m, 5H); HRMS (ESI), m/z, 200.0722; Anal. Calc. for $C_{13}H_{12}O_2$: C, 77.98; H, 6.04; Found: C, 77.94; H, 6.36.

1-(Benzyloxy)-4-(Octan-2-yloxy) Benzene, ***2***. This compound was prepared according to published procedures [17], as a white solid in 61% yield. ^{1}H NMR (ppm, $CDCl_3$): 0.84–0.98 (m, 3H), 1.24–1.77 (m, 13H), 4.16–4.26 (m, 1H), 5.01 (d, $J = 6.9$ Hz, 2H), 6.77–6.92 (m, 4H), 7.23–7.44 (m, 5H); HRMS (ESI), m/z, 345.2122; Anal. Calc. for $C_{21}H_{28}O_2$: C, 80.73; H, 9.03; Found: C, 80.67; H, 9.15.

4-(Octan-2-yloxy) Phenol, ***3***. A mixture of compound **2** (3.2 g, 9.4 mmol) was dissolved in THF (150 mL) containing a suspension of 10% Pd-C catalyst (1 g). The mixture was stirred under a hydrogen atmosphere at room temperature until no further hydrogen was taken up (ca. 10 h). The catalyst was removed by filtration through Celite and washed with an excess of THF (150 mL). The solvent

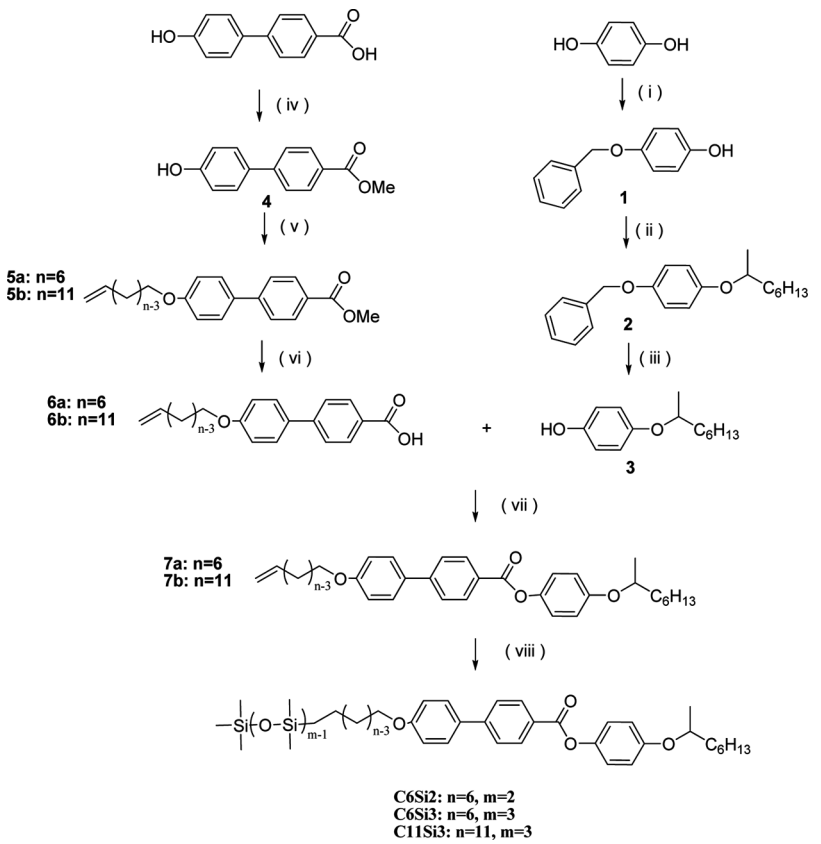

Scheme 1. Synthetic routes of intermediates and target molecules.

was removed by evaporation under reduced pressure and the crude product was purified by column chromatography on silica gel (chloroform/ethyl acetate, 50:1) to give a white solid in 93% yield. ^{1}H NMR (ppm, $CDCl_3$): 0.88 (t, $J = 6.6$ Hz, 3H), 1.24–1.87 (m, 13H), 4.09–4.23 (m, 1H), 4.53 (s, 1H), 6.72–6.85 (m, 4H); HRMS (ESI), m/z, 222.1523; Anal. Calc. for $C_{14}H_{22}O_2$: C, 75.63; H, 9.97; Found: C, 75.52; H, 10.06.

Methyl 4′-Hydroxybiphenyl-4-carboxylate, ***4.*** This compound was prepared according to published procedures [18], as a white solid in 95% yield. ^{1}H NMR (ppm, $CDCl_3$): 3.94 (s, 3H), 6.94 (d, $J = 8.7$ Hz, 2H), 7.54 (d, $J = 8.7$ Hz, 2H), 7.63 (d, $J = 8.4$ Hz, 2H), 8.09 (d, $J = 8.4$ Hz, 4H); HRMS (ESI), m/z, 228.0798; Anal. Calc. for $C_{14}H_{12}O_3$: C, 73.67; H, 5.03; Found: C, 73.78; H, 5.00.

Methyl 4′-(Hex-5-enyloxy)Biphenyl-4-carboxylate, ***5a.*** This compound was prepared according to published procedures [18], as a white solid in 62% yield. ^{1}H NMR (ppm, $CDCl_3$): 1.60 (m, 2H), 1.83 (m, 2H), 2.13 (m, 2H), 3.86 (s, 3H), 3.93–4.17 (m, 2H), 4.96–5.08 (m, 2H), 5.85 (m, 1H), 6.97 (m, 2H), 7.57 (m, 4H), 8.07 (d, $J = 6.0$ Hz, 2H); HRMS (ESI), m/z, 310.1582; Anal. Calc. for $C_{20}H_{22}O_3$: C, 77.39; H, 7.14; Found: C, 77.42; H, 7.12.

Methyl 4′-(Undec-10-enyloxy)Biphenyl-4-carboxylate, ***5b***. This compound was obtained from the reaction by using the similar procedure as described for compound **5a**. The product was isolated as a white solid in 60% yield. ^{1}H NMR (ppm, $CDCl_3$): 1.25–1.58 (m, 12H), 1.76–1.83 (m, 2H), 2.01–2.08 (m, 2H), 3.87 (s, 3H), 4.00 (t, $J = 6.0$ Hz, 2H), 4.91–5.03 (m, 2H), 5.75–5.88 (m, 1H), 6.97 (d, $J = 9.0$ Hz, 2H), 7.57 (d, $J = 9.0$ Hz, 2H), 7.62 (d, $J = 9.0$ Hz, 2H), 8.06 (d, $J = 9.0$ Hz, 2H); HRMS (ESI), m/z, 380.2415; Anal. Calc. for $C_{25}H_{32}O_3$: C, 78.91; H, 8.48; Found: C, 78.87; H, 8.47.

4′-(Hex-5-enyloxy) Biphenyl-4-carboxylic Acid, ***6a***. This compound was prepared according to published procedures [18], as a white solid in 87% yield. ^{1}H NMR (ppm, $CDCl_3$): 1.56 (m, 2H), 1.76 (m, 2H), 2.10 (m, 2H), 4.02 (t, $J = 6.3$ Hz, 2H), 4.94–5.07 (m, 2H), 5.77–5.89 (m, 1H), 7.05 (d, $J = 9.0$ Hz, 2H), 6.68 (d, $J = 9.0$ Hz, 2H), 7.50 (d, $J = 8.7$ Hz, 2H), 8.98 (d, $J = 8.4$ Hz, 2H), 12.88 (s, 1H); HRMS (ESI), m/z, 296.1398; Anal. Calc. for $C_{19}H_{20}O_3$: C, 77.00; H, 6.80; Found: C, 76.98; H, 6.77.

4′-(Undec-10-enyloxy) Biphenyl-4-carboxylic Acid, ***6b***. This compound was obtained from the reaction by using the similar procedure as described for compound **6a**. The product was isolated as a white solid in 90% yield. ^{1}H NMR (ppm, $CDCl_3$): 1.27–1.41 (m, 12H), 1.67–1.76 (m, 2H), 1.96–2.03 (m, 2H), 4.00 (t, $J = 6.3$ Hz, 2H), 4.90–5.02 (m, 2H), 5.71–5.85 (m, 1H), 7.04 (d, $J = 8.7$ Hz, 2H), 7.68 (d, $J = 9.0$ Hz, 2H), 7.75 (d, $J = 8.4$ Hz, 2H), 7.98 (d, $J = 8.4$ Hz, 2H), 12.89 (s, 1H); HRMS (ESI), m/z, 366.2168; Anal. Calc. for $C_{24}H_{30}O_3$: C, 78.65; H, 8.25; Found: C, 78.64; H, 8.11.

4-(Octan-2-yloxy) Phenyl 4′-(Hex-5-enyloxy)biphenyl-4-carboxylate, ***7a***. To a suspension of compounds **6a** (8.85 g, 29.9 mmol) and **3** (3.0 g, 13.6 mmol), dissolved in dry dichloromethane (100 ml), *N,N*-dicyclohexylcarbodiimide (DCC; 6.2 g, 29.9 mmol) and 4-(*N,N*-dimethylamino) pyridine (DMAP; 0.33 g, 2.72 mmol) were added to react under nitrogen. The reaction mixture was stirred for 12 h at room temperature. The precipitated dicyclohexylurea (DCU) was filtered off and washed with an excess of dichloromethane (50 mL). The filtrate was washed with water and dried over anhydrous magnesium sulfate. After removal of the solvent by evaporation under reduced pressure, the residue was purified by column chromatography on silica gel using chloroform as an eluent. The collected product was crystallized from a mixture of dichloromethane and 2-propanol to give **7a** as a white solid in 81% yield. ^{1}H NMR (ppm, $CDCl_3$): 0.89 (t, $J = 7.2$ Hz, 3H), 1.30–1.80 (m, 14H), 2.12–2.19 (m, 2H), 4.03 (t, $J = 6.6$ Hz, 2H), 4.30–4.36 (m, 1H), 4.97–5.08 (m, 2H), 5.78–5.91 (m, 1H), 6.99 (d, $J = 8.7$ Hz, 2H), 7.02 (d, $J = 8.7$ Hz, 2H), 7.13 (d, $J = 9.0$ Hz, 2H), 7.61 (d, $J = 8.7$ Hz, 2H), 7.70 (d, $J = 8.4$ Hz, 2H), 8.24 (d, $J = 8.7$ Hz, 2H); HRMS (ESI), m/z, 500.3022; Anal. Calc. for $C_{33}H_{40}O_4$: C, 79.16; H, 8.05; Found: C, 79.20; H, 8.03.

4-(Octan-2-yloxy)Phenyl 4′-(Undec-10-enyloxy)biphenyl-4-carboxylate, ***7b***. This compound was obtained from the reaction of compounds **3** and **6b** by using the similar procedure as descried for compound **7b**. The product was isolated as a white solid in 77% yield. ^{1}H NMR (ppm, $CDCl_3$): 0.89 (t, $J = 6.3$ Hz, 3H), 1.30–1.61 (m, 24H), 1.70–1.86 (m, 3H), 2.01–2.17 (m, 2H), 4.02 (t, $J = 6.3$ Hz, 2H), 4.30–4.36 (m, 1H), 4.92–5.03 (m, 2H), 5.77–5.89 (m, 1H), 6.94 (d, $J = 9.0$ Hz, 2H),

7.02 (d, $J = 8.7$ Hz, 2H), 7.13 (d, $J = 9.0$ Hz, 2H), 7.61 (d, $J = 8.7$ Hz, 2H), 7.70 (d, $J = 8.4$ Hz, 2H), 8.23 (d, $J = 8.4$ Hz, 2H); HRMS (ESI), m/z, 570.3665; Anal. Calc. for $C_{38}H_{50}O_4$: C, 79.96; H, 8.83; Found: C, 79.88; H, 8.93.

Target compounds were prepared by a similar method for that described for compound **C6Si2**. After workup, the crude products were purified by column chromatography on silica gel using toluene/ethyl acetate as an eluent and twice recrystallization from a mixture of 2-propanol as a white liquid crystal. The yields of these products after purification were ca. 82–87%.

4-(Octan-2-yloxy) Phenyl 4′-[6-(1,1,2,2,2-pentamethyldisiloxanyl)hexyloxy) Biphenyl-4-carboxylate, ***C6Si2***. Compound **7a** (0.11 mg, 0.225 mmol), 55 mg 1-hydropentamethyldisiloxane (0.25 mmol), and 0.6 mmol platinum divinyltetramethyldisiloxane as catalyst were dissolved in 5 mL of dry toluene in a flask fitted with a $CaCl_2$ drying tube. The reaction mixture was stirred at room temperature overnight. Column chromatography on silica gel with toluene/ethyl acetate gradient as eluant gave pure product. The collected product was crystallized from a mixture of 2-propanol to give **C6Si2** as a white liquid crystal in 82% yield. ^{1}H NMR (ppm, $CDCl_3$): 0.00–0.05 (s, 15H), 0.06–0.07 (m, 2H), 0.89 (t, $J = 7.0$ Hz, 3H), 1.30–1.55 (m, 19H), 1.81 (m, 2H), 4.02 (t, $J = 6.5$ Hz, 2H), 4.31–4.34 (m, 1H), 6.93 (d, $J = 9.0$ Hz, 2H), 7.01 (d, $J = 8.5$ Hz, 2H), 7.13 (d, $J = 9.0$ Hz, 2H), 7.60 (d, $J = 8.5$ Hz, 2H), 7.69 (d, $J = 8.5$ Hz, 2H), 8.22 (d, $J = 8.5$ Hz, 2H); HRMS (ESI), m/z, 648.3632; Anal. Calc. for $C_{38}H_{56}O_5Si_2$: C, 70.32; H, 8.70; Found: C, 70.31; H, 8.71.

4-(Octan-2-yloxy) Phenyl 4′-[6-(1,1,2,2,3,3,3-Heptamethyltrisiloxanyl)hexyloxy) Biphenyl-4-carboxylate, ***C6Si3***. The compound was prepared from **7a** and 1-hydroheptamethyltrisiloxane. The product was isolated as a white white liquid crystal in 84% yield. ^{1}H NMR (ppm, $CDCl_3$): 0.00–0.06 (s, 21H), 0.08–0.10 (m, 2H), 0.89 (t, $J = 7.0$ Hz, 3H), 1.30–1.55 (m, 19H), 1.82 (m, 2H), 4.02 (t, $J = 6.5$ Hz, 2H), 4.32–4.33 (m, 1H), 6.93 (d, $J = 9.0$ Hz, 2H), 7.01 (d, $J = 8.5$ Hz, 2H), 7.13 (d, $J = 9.0$ Hz, 2H), 7.60 (d, $J = 9.0$ Hz, 2H), 7.69 (d, $J = 8.5$ Hz, 2H), 8.23 (d, $J = 8.5$ Hz, 2H); HRMS (ESI), m/z, 722.3988; Anal. Calc. for $C_{40}H_{62}O_6Si_3$: C, 66.43; H, 8.64; Found: C, 66.20; H, 8.55.

4′-[11-(1,1,2,2,3,3,3-Heptamethyltrisiloxanyl) Undecyloxy) Biphenyl-4-carboxylate, ***C11Si3***. The compound was prepared from **7b** and 1-hydroheptamethyltrisiloxane. The product was isolated as a white white liquid crystal in 87% yield. ^{1}H NMR (ppm, $CDCl_3$): 0.00–0.01 (s, 21H), 0.06–0.07 (m, 2H), 0.89 (t, $J = 7.0$ Hz, 3H), 1.29–1.55 (m, 29H), 1.83 (m, 2H), 4.02 (t, $J = 6.5$ Hz, 2H), 4.32–4.34 (m, 1H), 6.93 (d, $J = 9.0$ Hz, 2H), 7.01 (d, $J = 9.0$ Hz, 2H), 7.13 (d, $J = 9.0$ Hz, 2H), 7.60 (d, $J = 9.0$ Hz, 2H), 7.69 (d, $J = 8.5$ Hz, 2H), 8.23 (d, $J = 8.5$ Hz, 2H); HRMS (ESI), m/z, 792.4458; Anal. Calc. for $C_{45}H_{72}O_6Si_3$: C, 78.13; H, 9.15; Found: C, 78.09; H, 9.09.

Results and Discussion

Thermal Properties and Optical Textures

The phase behaviors of all compounds were investigated by a combination of POM and DSC Phase transition temperatures observed by POM match well with the corresponding DSC thermograms. The mesomorphic properties of the studied

compounds **C6Si2**, **C6Si3**; and **C11Si3**; the phase sequence; phase transition temperatures; and enthalpy data are summarized in Table 1. Upon cooling from the isotropic state, the compound **C6Si2** displayed a characteristic Schlieren texture and broken fan textures of the mesophase at 86°C (see Fig. 1), indicating the formation of the SmC* phase. The other compounds **C6Si3** and **C11Si3** showed similar optical textures, thus implying that they have the same mesophase. All of the compounds exhibit enantiotropic mesomorphic behavior and only a mesophase. A typical DSC curve of compound **C6Si2** is shown in Fig. 2, which shows that one mesophase can be obtained and that there are no significant differences for different heating or cooling rates. In the DSC thermograms, the enthalpy values obtained for the SmC* mesophase to isotropic phase transition were in the range of about 4.16 to 5.58 kJ mol^{-1}.

A series of materials reported by Petrenko show that the inclusion of terminal siloxane at the end of the molecule increased steric hindrance between layers. Generally, the siloxane unit is also considered to be a microphase unit, but its size and flexibility disrupt the interlayer interface. As a result, when the structure adds more siloxane unit at the end, the clearing temperature of the compound is decreased. Comparison of compounds **C6Si2** and **C6Si3** upon cooling from the isotropic liquid shows that the compound **C6Si3** is due to the lowest clearing transition temperature. Thus, the size and flexibility effect of the siloxane unit have a profound influence on their mesomorphic behavior. Comparison of compounds **C6Si3** and **C11Si3**, shows that the clearing transition temperature is increased due to the increased achiral alkyl chain. The result also conforms to the previous reports.

XRD Studies

To further identify the type of mesophases, determination of structural parameters has been further performed by XRD. The theoretical molecular length of **C11Si3** determined from molecular model estimated using CS Chem3D Ultra 7.0 software gave molecular length of ca. 48.2 Å, where we suppose that the molecular structure

Table 1. Phase transition temperatures (°C) and enthalpies (kJ mol^{-1}; in parentheses) for the target compounds as determined by DSC (scan rate = 5°C min^{-1})[a]

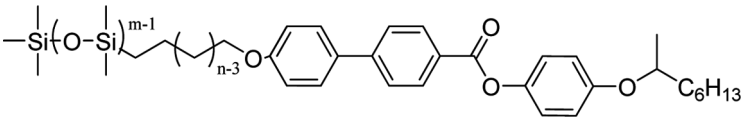

Compound	(n, m)	Cr	Second heating first cooling	SmC*	Second heating first cooling	I
C6Si2	(6, 2)	•	1.34 (+6.15) −7.20 (−5.92)	•	88.9 (+5.58) 87.5 (−5.56)	•
C6Si3	(6, 3)	•	>−30 >−30	•	65.8 (+4.16) 64.4 (−4.25)	•
C11Si3	(11, 3)	•	46.9 (+12.4) 32.8 (−10.5)	•	106.9 (+4.40) 105.4 (−4.19)	•

[a]Abbreviations: Cr = crystalline phase; SmC* = chiral SmC phase; I = isotropic phase (• = phase exists).

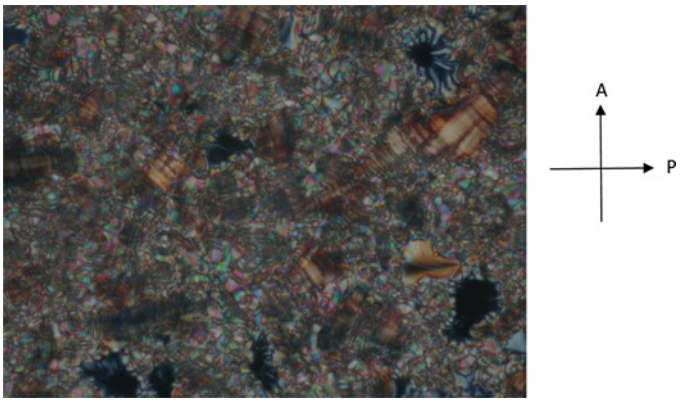

Figure 1. Polarized optical microscopic textures show Schlieren with broken fan-shaped textures in SmC* phase on cooling (1°C/min) from the isotropic state for compound **C6Si2** at 86°C.

is coplanar and the alkyl chains are fully extended in the all-*trans* conformation. As shown in Fig. 3a, the 2D diffraction pattern including two symmetric intense arcs in the small-angle region on the meridian XRD pattern of compound **C11Si3** and the data were integrated in Fig. 3b, as an illustrative example. The resulting XRD pattern of compound **C11Si3** at 100°C exhibits three Bragg reflections in the small-angle region at $2\theta = 1.96$, 3.92, and 5.88 with *d*-spacings of 39.9, 19.5, and 13.0 Å, respectively, corresponding to the reciprocal spacing in the ratios 1, 2, and 3, and to the indexation $(hk) = (10)$, (20), and (30), which implies the formation of a layered structure. On the other hand, a diffuse scattering halo in the wide-angle region centered at 2θ around 16.41° with *d*-spacing of ca. 4.6 Å indicates liquid-like arrangement of the molecules within the layers. As shown in Fig. 3c, the temperature dependence on the

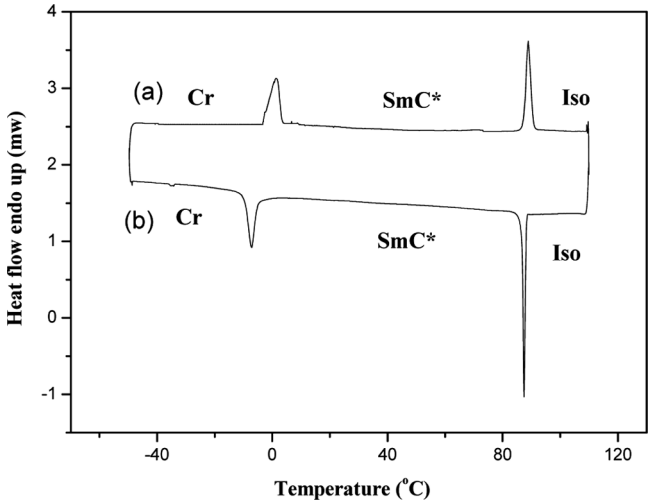

Figure 2. DSC curves of compound **C6Si2** obtained at a rate of 5°C min^{-1}: (a) second heating scan and (b) first cooling scan.

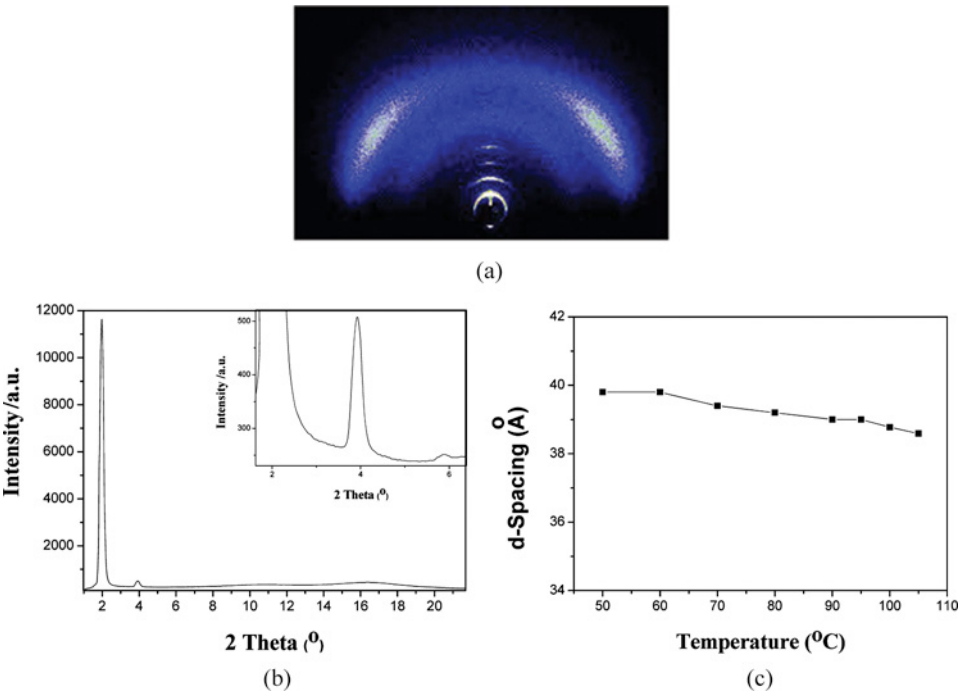

Figure 3. (a) 2D XRD pattern of a partially surface-aligned sample of compound **C11Si3** obtained in the SmC* phase at 100°C (upon cooling from the isotropic phase), (b) X-ray diffraction intensity against angle profile obtained in the SmC* phase of **(C11Si3)** at 100°C, and (c) layer *d*-spacing as a function of the temperature dependence (upon cooling from the isotropic phase).

layer *d*-spacing of compound **C11Si3** in the SmC* phase was recorded upon cooling from the isotropic phase. The values of the layer *d*-spacing only slightly change within the temperature range of the SmC* phase. Therefore, the layer *d*-spacing value of 39.9 Å for compound **C11Si3** by XRD measurement is smaller than the calculated theoretical molecular length of 48.2 Å, which suggests a tilted arrangement of smectic structure; that is, a smectic C phase with tilt angle of 34.1° along the layer normal direction. Compound **C6Si2** and **C6Si3** also revealed similar diffraction patterns at temperatures within the respective mesophase temperature range (see Table 2).

Electro-Optical Behavior

The switching behavior has been observed in the SmC* phase of the studied compound **C6Si2** using the triangular wave method. One distinct sharp peak per half period of an applied triangular wave voltage is clearly seen under a triangular wave field of about 80 Vpp at 60 Hz (see in Fig. 4a). This is a strong indication of a ferroelectric switching process. To clarify this, we also have measured the polarization by the Diamant-Bridge method (see Fig. 4b) and observed only single hysteresis loop down to the lowest frequency (1 Hz) available in the measurement, again indicating ferroelectric-type switching. The temperature dependence of the magnitude of the *P*s

Table 2. Summary data of target compounds

Compound	**C6Si2**	**C6Si3**	**C11Si3**
Mesophase	SmC*	SmC*	SmC*
Parameters (Å)	38.9	40.5	48.2
Measured spacings (Å)	29.7	30.8	39.9
Tilt angle (°)	40.2	40.5	34.1
Optical tilt angle (°)	45	41.5	44
Switching time (μs)[a]	23	141	35
Maximum *P*s/nC (cm^2)[a]	91	62	74

[a]The data were measured at $T_c - T = 20°C$.

value for the target compounds obtained by integrating the area under the one peak is shown in Fig. 4c. The abrupt increase of *P*s around the isotropization temperature indicates the phase transformation from the isotropic phase to the SmC* phase. It is also observed that the value of *P*s increases with decrease in temperature of the

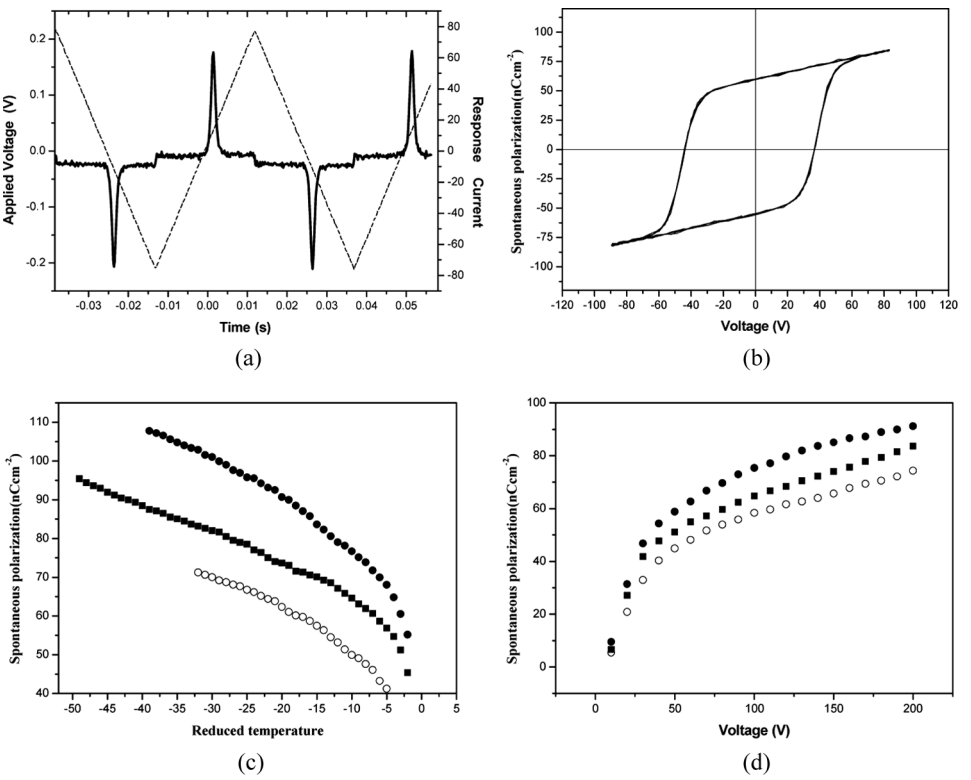

Figure 4. (a) Switching current response observed in the SmC* phase of compound **C6Si2** at 75°C under the applied triangular wave voltage (7.5 μm antiparallel rubbed polyimide-coated ITO cell, 80 Vpp, 60 Hz) and (b) bridge method. Summary of spontaneous polarization (*P*s) as a function of (c) the temperature and (d) voltage observed in the SmC* phase of target compounds (●: **C6Si2**; ○: **C6Si3**; ■: **C11Si3**).

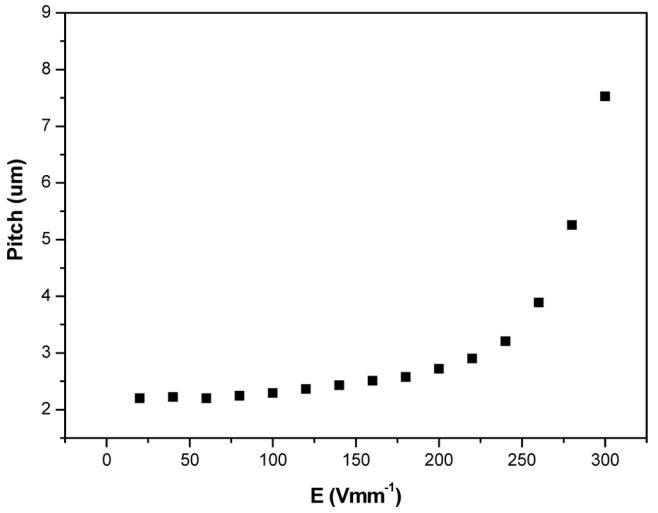

Figure 5. Helical pitch as a function of ac electric field in compound **C6Si2** at 80°C (f = 30 Hz).

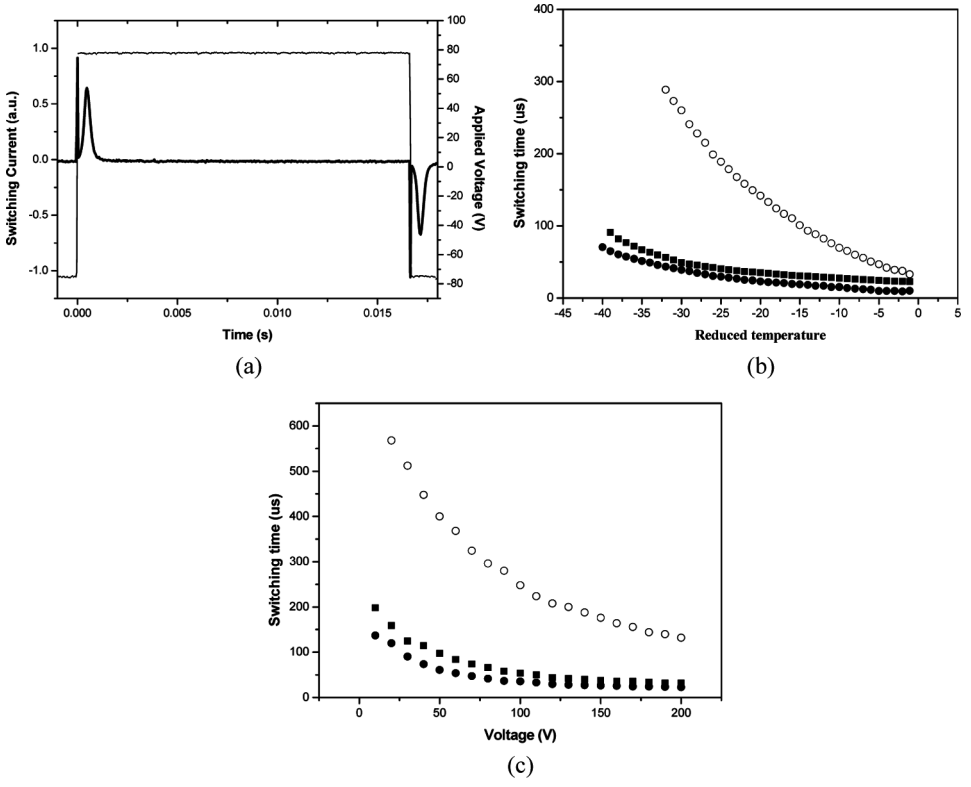

Figure 6. (a) The time dependences of the switching current under a square wave field for compound **C6Si2** at 30°C and (b) switching time as a function of temperature and (c) voltage for target compounds (on antiparallel rubbing direction LC cells with 7.5 μm thickness as Vpp = 150 V, f = 10 Hz;. ●: **C6Si2**; ○: **C6Si3**; ■: **C11Si3**).

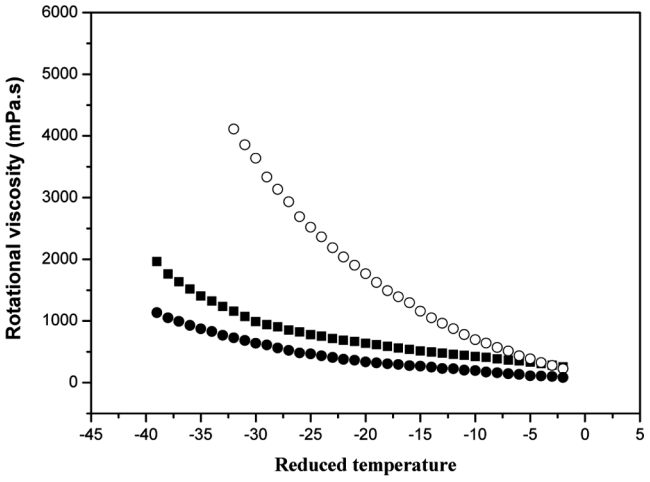

(a)

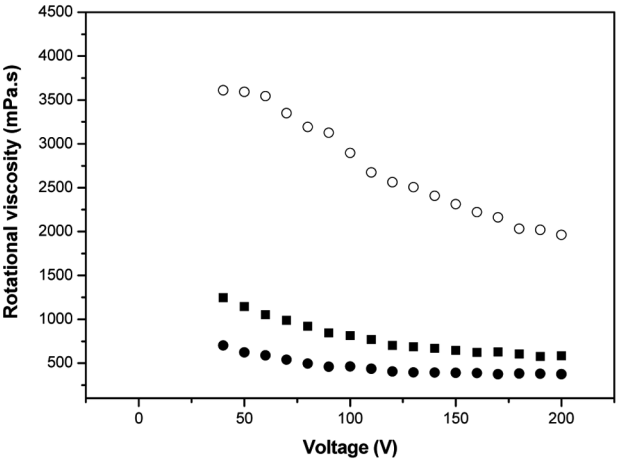

(b)

Figure 7. Behavior of rotational viscosity for target compounds with different (a) temperature and (b) voltage (●: **C6Si2**; ○: **C6Si3**; ■: **C11Si3**).

compounds. The increase in the *P*s value with decrease in the temperature may be due to the strong polarization-electric (P-E) field coupling and polarization-tilt angle (P-A) theta coupling [19]. We also see the behavior of spontaneous polarization with applied voltage, which is shown in Fig. 4d. Because the molecular helical order in the sample may not be suppressed completely by the confining substrates, it was observed that with an increase in the applied voltage, the spontaneous polarization increased sharply initially. The helix could be unwinding by applied field (see Fig. 5); result in such a dependence has been observed in FLC materials. However, the applied field may also induce a transition to a higher order phase that does not exist in the phase diagram without an applied field. The *P*s value exhibits a maximum polarization of $91\,\mathrm{nC\,cm^{-2}}$ for compound **C6Si2**, $62\,\mathrm{nC\,cm^{-2}}$ for compound **C6Si3**, and $74\,\mathrm{nC\,cm^{-2}}$ for compound **C11Si3** at $\mathrm{Tc} - \mathrm{T} = 20^{\circ}\mathrm{C}$ (see Table 2).

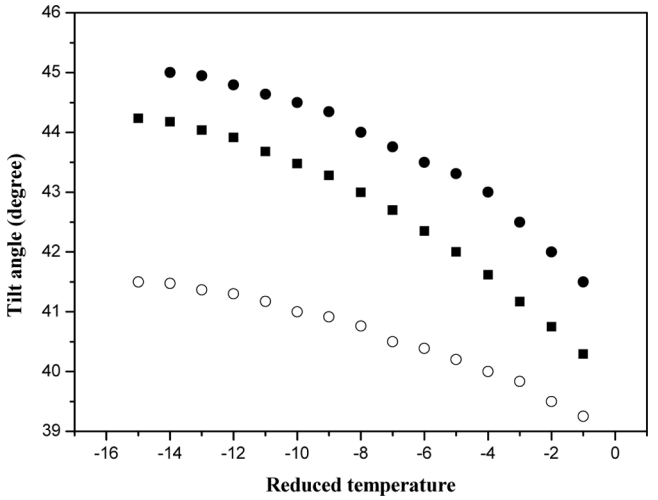

Figure 8. Tilt angle of the SmC* phase as a function of the dc electric fields in compounds (on antiparallel rubbing direction LC cells with 7.5 μm thickness) (**C6Si2**: ●; **C6Si3**: ○; **C11Si3**: ■).

Comparing, the spontaneous polarization value of target compounds (compounds, **C6Si3** and **C11Si3**), it appears that compounds with longer alkyl chain length have higher *P*s values at any temperature below the Curie point. It also seems that enable comparison of *P*s values for the length of the siloxane group (compounds **C6Si2** and **C6Si3**). It appears higher *P*s values with lower siloxane group length. The results also conform to previous reports [9].

In order to investigate the dynamics of the polarization switching behavior, the switching currents of compound **C6Si2** were measured with an applied square wave field (as Vpp = 80 V, f = 10 Hz) in the SmC* phase. The switching current curves of compound **C6Si2** at 30°C are shown in Fig. 6a as a function of time. The switching time (τ) values are determined from the time elapsed between the appearance of the maximum of the current signal and the field reversal. The switching time as a function of the temperature is shown in Fig. 6b (Vpp = 150 V, f = 10 Hz). The decrease of the switching time with increasing temperature for target compounds was observed due to the viscosity decrease. The switching time value of 23 μs for compound **C6Si2**, 141 μs for compound **C6Si3**, and 35 μs for compound **C11Si3** at Tc − T = 20°C was observed (see Table 2). The switching time with applied voltage has been shown in Fig. 6c. It was observed that the switching time decreases with increasing voltage.

The combined effect of the switching time and spontaneous polarization can be seen in the behavior of the rotational viscosity, as shown in Fig. 7a and Fig. 7b. These three are related with each other by the following relation

$$\gamma_\psi = \tau P_S E \tag{1}$$

where τ is switching time, γ_ψ is the rotational viscosity, *Ps* is the spontaneous polarization, and E is the applied field. The rotational viscosity decreases, the spontaneous polarization increases, and the switching time decreases in accordance with Eq. (1). The rotational viscosity value of 336 mPass for compound **C6Si2**,

1, 766 mPass for compound **C6Si3**, and 640 mPass for compound **C11Si3** at Tc – T = 20°C were exhibited (Vpp = 150 V, f = 10 Hz).

The optical tilt angles for all compounds in the SmC* phase were measured as a function of temperature on cooling. The measured optical tilt angle as a function of temperature for the SmC* phase for target compounds shown in Fig. 8 enables comparison of optical tilt angles with different lengths of the alkyl chain and different lengths of the siloxane group in the tail of the compounds. In general, the optical tilt angles increase with decreasing temperature and exhibit a maxima. The maximum optical angles for the three compounds are similar at any temperature below the Curie point. The tilt angle value exhibits a maximum of 45° for compound **C6Si2**, 44° for compound **C6Si3**, and 41.5° for compound **C11Si3** at Tc – T = 20°C.

The temperature and frequency dependence of the dielectric constant for **C11Si3** is shown in Fig. 9a. For **C11Si3**, the dielectric constant increased sharply at the Iso-SmC* phase transition region. The maximum value of the dielectric constant was observed near the Iso-SmC* phase. As the temperature decreased, the dielectric constant decreased slightly, corresponding to the increase of the tilt angle in the

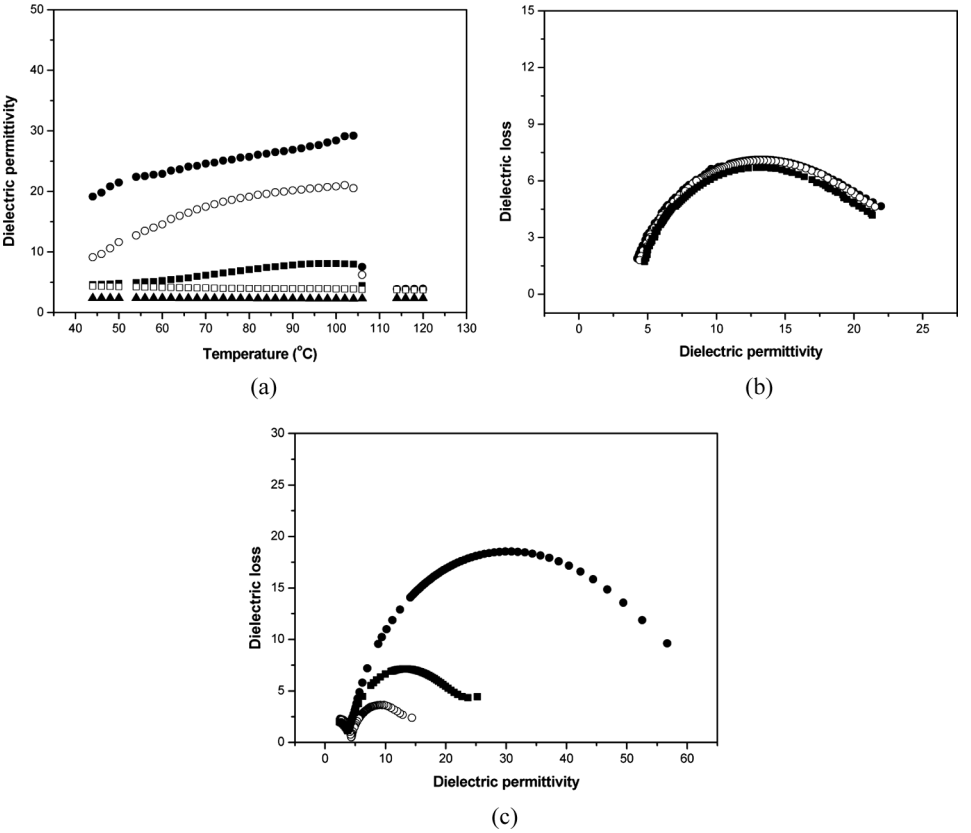

Figure 9. (a) Temperature dependence of the dielectric constant (ε') at 10^2 (●), 10^3 (○), 10^4 (■), 10^5 (□), and 10^6 (△) Hz for **C11Si3**. (b) Cole-Cole plot for **C11Si3** at different temperatures: 85°C (●), 70°C (○), and 50°C (■). (c) Cole-Cole plot of the dielectric permittivity in the SmC* phase of target compounds at Tc – T = 15°C (**C6Si2**: ●; **C6Si3**: ○; **C11Si3**: ■).

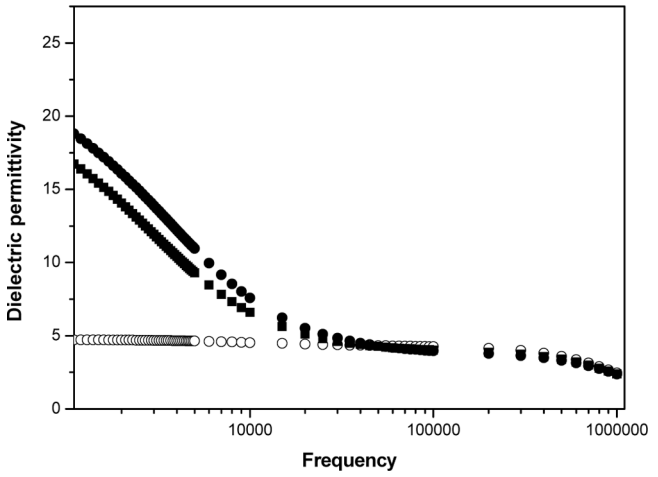

Figure 10. Dielectric permittivity (ε') as a function of log of frequency at 0 V (●) and 35 V (○) and again at 0 V (■) for compound **C11Si3**.

SmC* phase. The molecules have such a large tilt angle that their rotational freedom is decreased somewhat by steric hindrance [20]. This result would cause the molecular motion (Goldstone mode) to decrease. The Cole-Cole plot (ϵ'' *versus* ϵ'') provides valuable information with regard to the dielectric relaxation process. Almost semicircular Cole-Cole plots at various temperatures are shown in Fig. 9b for the γ relaxation of **C11Si3**. The relaxation strength (diameter of the circle) is similar with increasing temperature. The Cole-Cole plot of the dielectric permittivity in the SmC* phase of target compounds at $Tc - T = 15°$**C** was observed (see Fig. 9c). As a result, the relaxation strength increased with decreasing length of the achiral terminal chain. Figure 10 shows the dielectric permittivity as function of frequency in **C11Si3**. As can be seen from the figure, with the change in bias voltage of the measuring field from 0 to 35 V, the permittivity value decreases to a minimum, which is due to suppression of the phason (Goldstone) mode, which occurs due to phase fluctuation of the molecules [21]. But again taking measurements at zero bias, the sample cell shows small memory effects.

Conclusions

We have achieved the molecular design, synthesis, and characterization of liquid crystals with a 4-hydroxyphenyl 4′-hydroxybiphenyl-4-carboxylate core, chiral octan-2-ol unit, and oligomeric siloxane end-group. Specifically, we have explored the possibility of stabilizing a wide thermal range chiral smectic C (SmC*) phase. It exhibits the SmC* phase over 100°C thermal range. Electro-optic studies were carried out for the majority of the compounds exhibiting the SmC* phase. Electrical switching and molecular tilt angle as functions of temperature and voltage were investigated in the SmC* phase. The tilt angle of **C6Si2** compound can reach up to 45° at high fields (160 V) in the SmC* phase, and the response time range was between 23 μs at 160 V in SmC*. The tilt angle, dielectric behavior, and switching property appearing in the SmC* phase of the target compounds were observed.

Acknowledgment

We thank Dr. Jey-Jau Lee for help with the XRD experiments at National Synchrotron Radiation Research Center (NSRRC, for the beamline BL17A) in Taiwan. Financial support from the National Science Council of Taiwan (ROC) through 98-2221-E-011-004 is gratefully acknowledged.

References

[1] Wu, S. L., & Hsu, H. N. (2007). *Liq. Cryst.*, *34*, 1159.
[2] Yoshizawa, A., Nishiyama, I., Fukumasa, M., Hirai, T., & Yamane, M. (1989). *Jpn. J. Appl. Phys.*, *28*, 1269.
[3] Coles, H. J., Owen, H., Newton, J., & Hodge, P. (1993). *Liq. Cryst.*, *15*, 737.
[4] Sunohara, K., Takatoh, K., & Sakamoto, M. (1993). *Liq. Cryst.*, *13*, 283.
[5] Newton, J., Coles, H., Hodge, P., & Hannington, J. (1994). *J. Mater Chem.*, *4*, 869.
[6] Poths, H., Wischerhoff, E., Zentel, R., Schonfeld, A., Henn, G., & Kremer, F. (1995). *Liq. Cryst.*, *18*, 811.
[7] Sun, Z. M., Zhang, X., & Feng, D. (1990). *Europhys. Lett.*, *11*, 415.
[8] Ibn-Elhaj, M., Skoulios, A., Guillon, D., Newton, J., Hodge, P., & Coles, H. J. (1996). *J. Phys. II*, *6*, 271.
[9] Corsellis, E., Guillon, D., Kloess, P., & Coles, H. (1997). *Liq. Cryst.*, *23*, 235.
[10] Robinson, W. K., Carboni, C., Kloess, P., Perkins, S. P., & Coles, H. J. (1998). *Liq. Cryst.*, *25*, 301.
[11] Naciri, J., Ruth, J., Crawford, G., Shashidhar, R., & Ratna, B. R. (1995). *Chem. Mater.*, *7*, 1397.
[12] Naciri, J., Shenoy, D. K., Keller, P., Gray, S., Crandall, K., & Shashidhar, R. (2002). *Chem. Mater.*, *14*, 5134.
[13] Vlahakis, J. Z., Maly, K. E., & Lemieux, R. P. (2001). *J. Mater. Chem.*, *11*, 2459.
[14] Marzec, M., Mikulko, A., Wrobel, S., Dabrowski, R., Darius, M., & Haase, W. (2004). *Liq. Cryst.*, *31*, 153.
[15] Diamant, H., Drenck, K., & Pepinsky, R. (1957). *Rev. Sci. Instrum.*, *28*, 30.
[16] Raina, K. K., & Kumar, P. (2009). *Journal of the Indian Institute of Science*, *89*(2), 243.
[17] Brunsveld, L., Zhang, H., Glasbeek, M., Vekemans, J. M., & Meijer, E. W. (2000). *J. Am. Chem. Soc.*, *122*, 6175.
[18] Olsson, N., Helgee, B., Andersson, G., & Komitov, L. (2005). *Liq. Cryst.*, *32*, 1139.
[19] Raina, K. K., & Kumar, P. (2009). *J. Indian Inst. Sci.*, *89*(2), 243.
[20] Krone, V., & Ringsdorf, H. (1991). *Liq. Cryst.*, *9*, 207.
[21] Hiller, S., Biradar, A. M., & Haase, W. (1996). *Phys. Rev. E*, *53*, 641.